Correlation between antiferromagnetic and Mott states in spin orbit coupled Sr_2IrO_4: A study of $Sr_2Ir_{1-x}M_xO_4$ ($M =$ Fe or Co)

Bing Hu [1,2] Hengdi Zhao,[1] Yu Zhang,[1] Pedro Schlottmann,[3] Feng Ye,[4] and Gang Cao [1,*]

[1]*Department of Physics, University of Colorado at Boulder, Boulder, Colorado 80309, USA*
[2]*School of Mathematics and Physics, North China Electric Power University, Beijing 102206, China*
[3]*Department of Physics, Florida State University, Tallahassee, Florida 32306, USA*
[4]*Neutron Scattering Division, Oak Ridge National Laboratory, Oak Ridge, Tennessee 37831, USA*

Sr_2IrO_4 is an archetypal spin-orbit-coupled Mott insulator with an antiferromagnetic state below 240 K. Here we report results of our study on single crystals of $Sr_2Ir_{1-x}Fe_xO_4$ ($0 \leqslant x < 0.32$) and $Sr_2Ir_{1-x}Co_xO_4$ ($0 \leqslant x < 0.22$). Fe doping retains the antiferromagnetic state but simultaneously precipitates an emergent metallic state whereas Co doping causes a rapid collapse of both the antiferromagnetic and Mott states, giving rise to a confined metallic state featuring a pronounced linearity of the basal-plane resistivity up to 700 K. The results indicate tetravalent $Fe^{4+}(3d^4)$ ions in the intermediate spin state with $S = 1$ and $Co^{4+}(3d^5)$ ions in the high spin state with $S = 5/2$ substituting for $Ir^{4+}(5d^5)$ ions in Sr_2IrO_4, respectively. The effective magnetic moment closely tracks the Néel temperature as doping increases, suggesting that the spin state of the dopant predominately determines the magnetic properties in doped Sr_2IrO_4. Furthermore, all relevant properties including charge-carrier density (e.g., $10^{28}/m^3$), Sommerfeld coefficient (e.g., 19 mJ/mole K^2), and Wilson ratio (e.g., 2.6) consistently demonstrate an emergent metallic state that is both robust and highly correlated in the two systems, arising from the percolation of bound states and the weakening of structural distortions. This study strongly indicates that the antiferromagnetic and Mott states are correlated in an unconventional manner in Sr_2IrO_4.

I. INTRODUCTION

The spin-orbit-coupled Mott state in Sr_2IrO_4 is an intriguing consequence of a delicate interplay of on-site Coulomb repulsion U, strong spin-orbit interactions (SOI), and crystalline field effects [1–8]. The iridate is among the most extensively studied quantum materials in recent years in part because of its apparent structural and magnetic similarities to those of the cuprate La_2CuO_4 and the widely anticipated superconductivity in electron-doped Sr_2IrO_4 [9–14], which, however, has remained elusive thus far. This conspicuous absence of the anticipated superconductivity brings to light an underappreciated nature of the spin-orbit-coupled Mott state, making Sr_2IrO_4 even more interesting and extraordinary for further investigations.

Sr_2IrO_4 adopts a canted antiferromagnetic (AFM) state [15] with a Néel temperature $T_N = 240$ K [16–19] and an energy gap $\Delta \leqslant 0.62$ eV [20–22]. Empirical trends indicate that the iridate lacks a conventional correlation between the magnetic and insulating states, that is, the AFM order does not always track changes of the insulating state in Sr_2IrO_4 [5]. Recent studies show that the insulating state in Sr_2IrO_4 unusually persists at megabar pressures up to 185 GPa [23], and yet the AFM state already diminishes at 17 GPa [24], which inspires expectations of pressured-induced quantum

paramagnetism [25] and an exotic insulating state [23]. In contrast, the ground state of the iridate is far more susceptible to impurity doping. Oftentimes, a slight substitution at either the Sr^{2+} site (e.g., La^{3+}, Ca^{2+}, and Ba^{2+}) [26–28] or the Ir^{4+} site (e.g., Mn^{3+}, Ru^{4+}, Rh^{3+} or Rh^{4+}, and Tb^{4+}) [29–39] causes disproportionately large changes in either the insulating state or the magnetic state or both. However, each dopant mentioned above generates unique, quite often exotic behavior in its own right, implying a rich phase diagram of the spin-orbit-coupled Mott state that is yet to be fully explored and understood.

In this paper, we report results of our study on single crystals of Fe and Co doped Sr_2IrO_4 or $Sr_2Ir_{1-x}Fe_xO_4$ ($0 \leqslant x < 0.32$) and $Sr_2Ir_{1-x}Co_xO_4$ ($0 \leqslant x < 0.22$). The key observations are that Fe doping preserves the AFM state but simultaneously precipitates an emergent metallic state; in contrast, Co doping causes a rapid collapse of both the AFM and Mott states, giving rise to a highly anisotropic or confined metallic state that features a pronounced linearity of the basal-plane resistivity extending up to 700 K with no sign of saturation. The detailed experimental results including structural, transport, thermal, and magnetic properties indicate that it is tetravalent $Fe^{4+}(3d^4)$ and $Co^{4+}(3d^5)$ ions that substitute tetravalent $Ir^{4+}(5d^5)$ ions in Sr_2IrO_4, respectively. The crystalline field of the octahedra splits the $3d$ states into a t_{2g} ground-triplet and an excited e_g doublet. Hence, the crystalline field splitting quenches the angular momentum and competes with the Hund exchange that tends to maximize the spin in

*gang.cao@colorado.edu

the $3d$ ion. Three spin states are possible for both Fe^{4+} and Co^{4+}, namely a high-spin state (HS), an intermediate spin state (IS), and a low-spin state (LS). For Fe^{4+} these states have spin $S = 2$, $S = 1$, and $S = 0$, respectively, while for Co^{4+} the spins are $S = 5/2$, $3/2$, and $1/2$. Since Hund's rules are local interactions, the underlying SOI environment in the iridates plays only a secondary role for the impurities. The effective moment of the compounds grows with increasing doping, for both Fe^{4+} and Co^{4+}. The Néel temperature in the Fe compound is not affected up to $x = 0.2$, but T_N drops rapidly with increasing Co substitution. All the results indicate that the spin state of the dopant predominately determines the magnetic properties in doped Sr_2IrO_4.

Furthermore, an array of significantly enhanced characteristic parameters, such as charge-carrier density (10^{27}, $10^{28}/m^3$), Sommerfeld coefficient (30, 19 mJ/mole K^2), and Wilson ratio (2.7, 2.6), consistently demonstrates a metallic state that is both robust and highly correlated in $Sr_2Ir_{1-x}Fe_xO_4$ and $Sr_2Ir_{1-x}Co_xO_4$. In these materials, the $Fe^{4+}(3d^4)$ ions offer additional holes leading to hydrogenlike acceptor states of large Bohr radius, which rapidly percolate into an impurity band with increasing x. On the other hand, the neutral substitution of $Co^{4+}(3d^5)$ ions adds neither holes nor electrons but breaks the translational invariance of the lattice leading to a small bound state of the size of a unit cell [40]. Both impurities locally reduce the SOI effect of the undoped iridate [1] and significantly relax the structural distortions inherent in Sr_2IrO_4. This study underscores that the AFM and insulating states coexist in an unconventional manner in Sr_2IrO_4, which sharply contrasts situations in other correlated materials such as La_2CuO_4, whose hallmark is a strong correlation between the AFM and Mott states. Note that synthesis and magnetic characterization of Fe and Co doped Sr_2IrO_4 in polycrystalline form were reported in Ref. [41]. For clarification, we point out that our data are in general agreement with the change of T_N in Fe doped Sr_2IrO_4 reported in Ref. [41], but inconsistent with the results of Co doped Sr_2IrO_4 reported in Ref. [41], which shows no change in T_N up to $x = 0.10$.

II. EXPERIMENT

Single crystals of Fe or Co doped Sr_2IrO_4 were grown using a flux method. The starting materials were $SrCO_3$, $SrCl_2$, IrO_2, and Fe_2O_3 or Co_3O_4. The mixtures were fired in Pt crucibles at 1440 °C for 15 h and then slowly cooled to room temperature at a rate of 3 °C/h. Measurements of crystal structures were performed using a Bruker Quest ECO single-crystal diffractometer equipped with a PHOTON 50 CMOS detector. It is also equipped with an Oxford Cryosystem that creates sample temperature environments ranging from 80 to 400 K during x-ray diffraction measurements. Chemical analyses of the samples were performed using a combination of a Hitachi MT3030 Plus scanning electron microscope and an Oxford energy dispersive x-ray spectroscopy (EDX). Magnetic properties were measured using a Quantum Design (QD) MPMS-XL superconducting quantum interference device magnetometer. The measurements of the electrical resistivity and Hall effect were carried out using a QD Dynacool PPMS System equipped with a 14-T magnet and a dilution

refrigerator. High temperature resistivity up to 700 K was measured using a home-made setup. The heat capacity was measured down to 0.05 K using a dilution refrigerator for the PPMS.

III. RESULTS AND DISCUSSION

A. Structural properties

The dopant Fe or Co substitutes Ir with a doping level up to 32% and 22%, respectively. The Fe or Co doping retains the native crystal structure but significantly alters the lattice parameters of $Sr_2Ir_{1-x}M_xO_4$ (M = Fe or Co), as shown in Fig. 1. A remarkable trend is that the unit cell volume V shrinks with increasing x; specifically, V is smaller by 0.46% and 0.48% at $x = 0.31$ of Fe doping and $x = 0.17$ of Co doping, respectively, compared to V for $x = 0$ [Fig. 1(f)]. The reduction of V, along with a shortening of the basal-plane bond length Ir-O2 [Figs. 1(b) and 1(g)], indicates that the ionic radius of the dopant, Fe or Co, must be smaller than that of the Ir^{4+} ($5d^5$) ion. Of all possible oxidation states of the Fe and Co ions, it is most likely that the Fe^{4+} ($3d^4$) or Co^{4+} ($3d^5$) ion substitutes the Ir^{4+} ion in Sr_2IrO_4 because the ionic radius r of both Fe^{4+} and Co^{4+} ions is smaller than that of the Ir^{4+} ion, i.e., $r(Ir^{4+}) = 0.625$ Å $> r(Fe^{4+}) = 0.585$ Å $> r(Co^{4+}) = 0.530$ Å. That $r(Co^{4+})$ is smaller than $r(Fe^{4+})$ explains the more rapid reduction in V with Co doping, consistent with the empirical Vegard's law [Fig. 1(f)]. This argument rules out possibilities of lower oxidation states of Fe and Co because due to the screened Coulomb potential of the nucleus the ionic radius is a strong function of the oxidation state, decreasing as d electrons are removed, that is, the lower the oxidation state an ion has, the larger the ionic radius of the ion becomes. For example, $r[Fe^{3+}(3d^5)] = 0.645$ Å $> r[Fe^{4+}(3d^4)]$, and $r[Co^{3+}(3d^6)] = 0.610$ Å $> r[Co^{4+}(3d^5)]$. Note that $r(Co^{3+})$ is slightly smaller than $r(Ir^{4+})$ ($= 0.625$ Å), but the rapid and significant volume reduction due to Co doping, e.g., $\Delta V/V = 0.48\%$ at $x = 0.17$ (compared to 0.46% at $x = 0.31$ of Fe doping), makes the Co^{3+} ion an unlikely replacement for Ir^{4+} in Sr_2IrO_4. This point is also corroborated by the sizable shortening of the basal-plane bond length Ir-O2 [Fig. 1(g)].

In short, the above structural analysis leads to the assignment of oxidation state of Fe^{4+} ($3d^4$) and Co^{4+} ($3d^5$). This means that an Fe^{4+} ion with four $3d$ electrons provides hole doping whereas a Co^{4+} ion with five $3d$ electrons offers no additional holes or electrons in Sr_2IrO_4.

Moreover, the chemical doping also lessens structural distortions inherent in Sr_2IrO_4 as the Ir-O-Ir bond angle [Fig. 1(b)] relaxes with increasing x [Fig. 1(h)], indicating that the Fe or Co dopant significantly reduces the rotation of octahedral IrO_6, which plays an important role in determining the physical properties [5,6,15,42,43].

B. Magnetic properties

We now examine the magnetic properties of $Sr_2Ir_{1-x}Fe_xO_4$ and $Sr_2Ir_{1-x}Co_xO_4$ illustrated in Fig. 2.

$Sr_2Ir_{1-x}Fe_xO_4$. One striking observation is that Fe doping up to 20% essentially retains the native Néel temperature T_N. Both the a-axis and c-axis magnetization, $M_a(T)$ and $M_c(T)$,
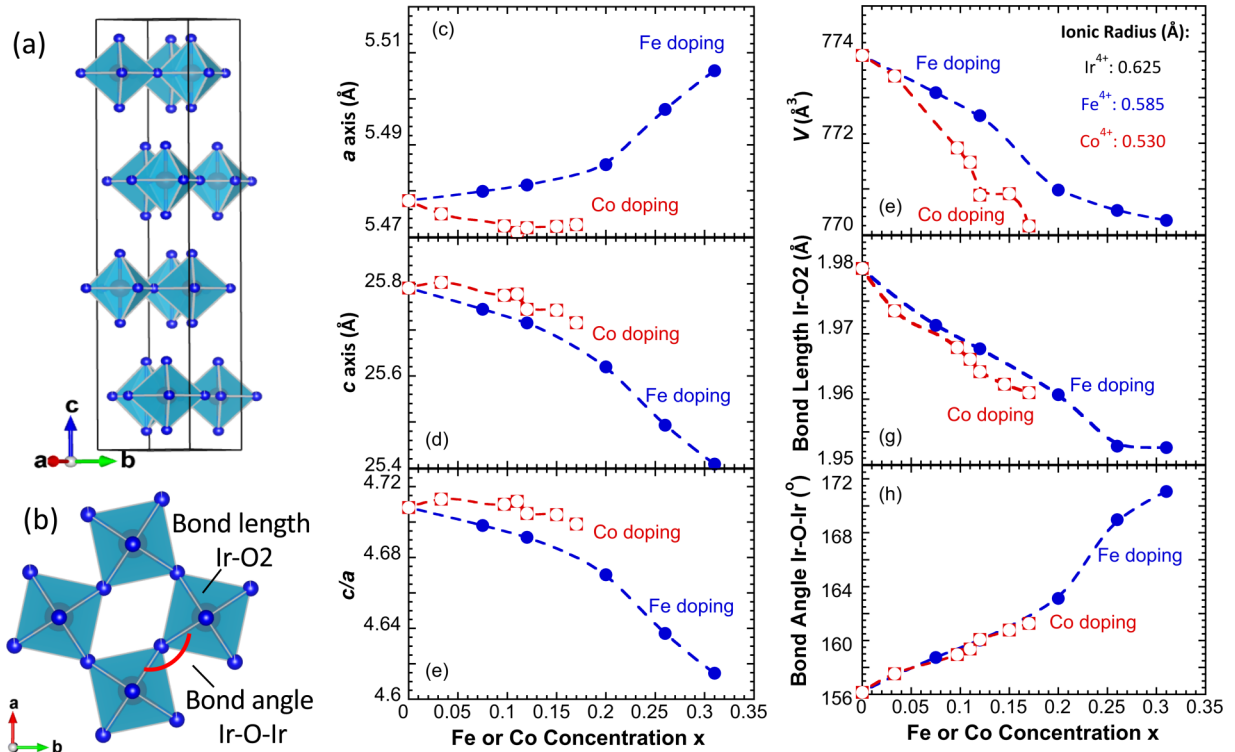
FIG. 1. Structural properties of $Sr_2Ir_{1-x}Fe_xO_4$ and $Sr_2Ir_{1-x}Co_xO_4$ at 100 K: (a) the unit cell of Sr_2IrO_4; (b) the basal plane of Sr_2IrO_4. The x dependence of (c) the a axis, (d) the c axis, (e) the ratio of c/a, (f) the unit cell volume V, (g) the bond length Ir-O2, and (h) the bond angle Ir-O-Ir.

exhibit little shift in T_N for $x \leqslant 0.18$, as shown in Figs. 2(a) and 2(b). The Fe dopant sharply contrasts other dopants on the Ir site, such as Rh, Mn, Tb [29–32,35–39], and Co, that readily suppress the AFM order; but it hints certain similarity to Ru doping discussed below [33,34]. The temperature dependence of $M_a(T)$ and $M_c(T)$ changes significantly below T_N. A rapid rise in $M_a(T)$ and $M_c(T)$ below 35 K, T^*, whose onset is defined by the valley in M, is likely a result of the polarization of the acceptor states; it gets stronger in magnitude and shifts to higher temperatures with increasing x [Figs. 2(a) and 2(b)]. The upturn of $M(T)$ and the slow increase of μ_{eff} with x [Fig. 2(c)] are an indication that Fe^{4+} is in the intermediate spin state, $S = 1$. The low T magnetic anomaly is not a phase transition because no corresponding anomaly around T^* is seen in the heat capacity discussed below. In addition, the magnetic anisotropy between $M_a(T)$ and $M_c(T)$ becomes increasingly weaker as x increases [Figs. 2(a) and 2(b)], which appears consistent with the shortening of the c axis [Fig. 1(d)], thus an enhanced interplane magnetic interaction.

Furthermore, the isothermal magnetization $M(H)$ increases considerably with x but becomes less "saturated," compared to that in $x = 0$ [see inset in Fig. 2(b)], suggesting a reduced magnetic canting, which produces the weak ferromagnetic behavior that features $x = 0$. Since the magnetic moment is strongly coupled to the lattice [5,6,15,42,43], a relaxed Ir-O-Ir bond angle [Fig. 1(h)] inevitably weakens the Dzyaloshinskii-Moriya interaction that drives magnetic canting, thus weak ferromagnetism. A change in the magnetic configuration is possible, and is seen in Mn, Rh, or Ru doped Sr_2IrO_4 [30,32,34].

More data analysis using a Curie-Weiss law retrieves the Curie-Weiss temperature θ_{CW} and effective moment μ_{eff} which deserves a close examination. θ_{CW} slowly decreases with x for $x < 0.20$. For example, θ_{CW} is merely reduced to 213 K for $x = 0.14$ from 250 K for $x = 0$, as shown in a $\Delta\chi^{-1}$ plot in Fig. 2(a) (note that χ is the magnetic susceptibility; $\Delta\chi = \chi - \chi_0$, where χ_0 is the temperature-independent contribution to χ). θ_{CW} essentially tracks T_N [Fig. 2(c)] as a function of x, dropping precipitously only when $x > 0.20$. Clearly, the superexchange interaction between magnetic moments supporting the AFM order is surprisingly resilient to Fe doping up to 20%.

This intriguing behavior calls for an understanding. As established above, the Fe^{4+} ion carries four $3d$ electrons with a less than half filled $3d$ shell. Accordingly, the first Hund's rule dictates the total spin to be $S = 1$ (the d_{xy} is doubly occupied, while the d_{xz} and d_{yz} orbitals have one electron) and the orbital angular momentum is quenched by the crystalline field. Since for $x = 0$ $\mu_{eff} = 0.46\mu_B/f.u.$ and the Fe ions contribute with $S = 1$, the effective moment μ_{eff} only rises slightly to $0.67\mu_B/f.u.$ for $x = 0.14$, as shown in Fig. 2(c). Such a small increase in μ_{eff} for $x \leqslant 0.14$ implies that the Fe ions are in the $S = 1$ state, thus contributing a very small amount of magnetic moment to the total value of μ_{eff}. As the Fe doping level further increases, the acceptor bound states start to overlap forming a band which allows the Fe spins to interact with each other giving rise to ferromagnetic correlations. This explains a rapid rise in μ_{eff} for $x > 0.20$, where μ_{eff} increases to $1.90\mu_B/f.u.$ for $x = 0.22$ and then to $2.73\mu_B/f.u.$ for $x = 0.31$ [Fig. 2(c)].

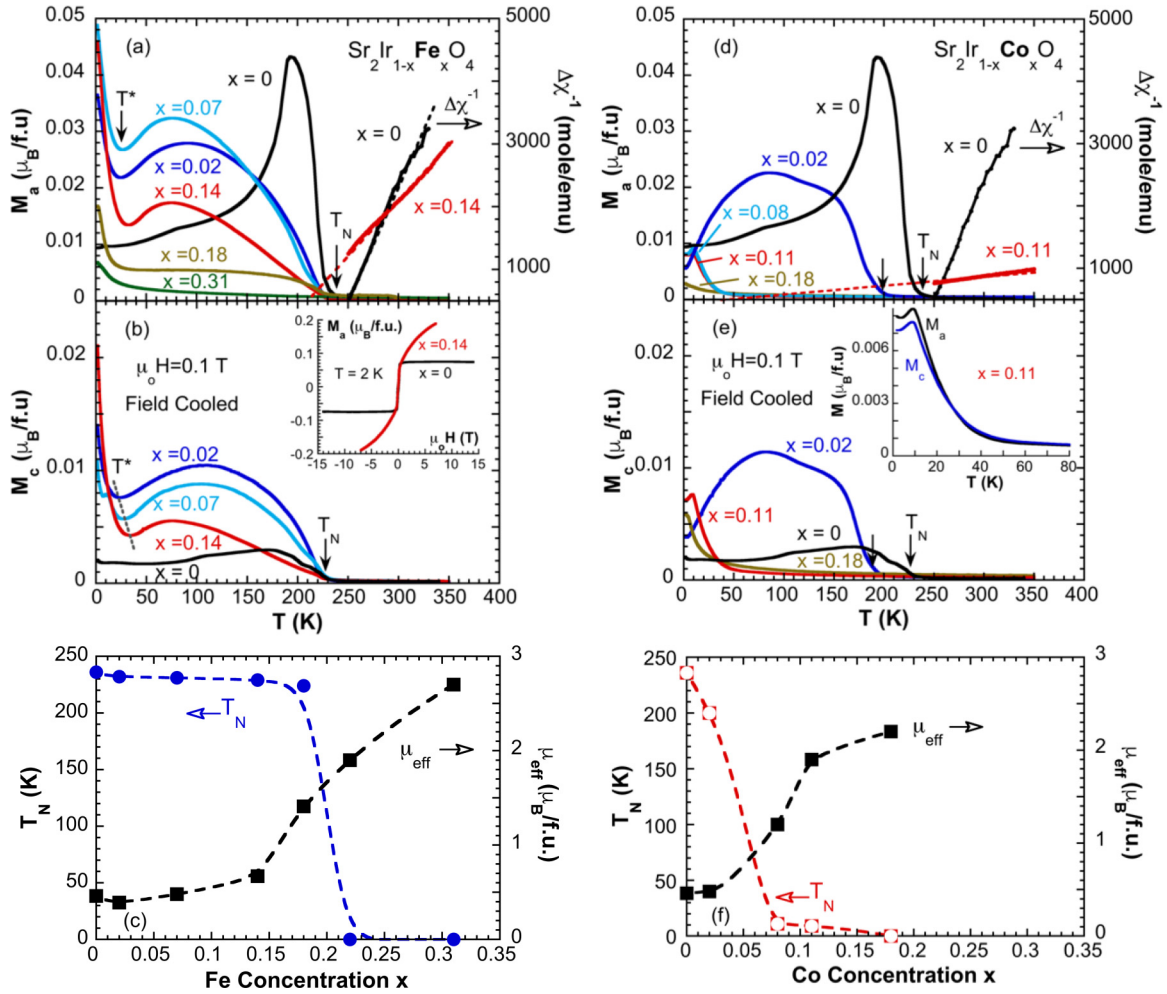FIG. 2. Magnetic properties of Sr_2Ir_{1-x}**Fe**$_xO_4$ and Sr_2Ir_{1-x}**Co**$_xO_4$: Temperature dependence of (a) the a-axis magnetization M_a and (b) the c-axis magnetization M_c for Sr_2Ir_{1-x}**Fe**$_xO_4$; (c) the Néel temperature T_N (left scale) and the effective moment μ_{eff} (right scale) as a function of Fe doping x. Temperature dependence of (d) the a-axis magnetization M_a and (e) the c-axis magnetization M_c for Sr_2Ir_{1-x}**Co**$_xO_4$; (f) the Néel temperature T_N (left scale) and the effective moment μ_{eff} (right scale) as a function of Co doping x. Note that the dashed line in (b) is a guide for the eye, indicating the shifting $T*$.

It is thus almost certain that the unexpected resilience of the AFM order to the Fe doping for $x < 0.20$ is primarily because the Fe^{4+} ions have only a $S = 1$ spin, thus carrying essentially small magnetic moments that are too weak to effectively affect the superexchange interaction of the iridate and thus the AFM order. With further increasing Fe doping ($x > 0.20$), the SOI weakens in the host and the Fe magnetic moments eventually become strong enough to suppress T_N when $x > 0.2$. That T_N and μ_{eff} closely track each other in an opposite fashion with increasing x reinforces this argument, as evidenced in Fig. 2(c). A strikingly similar trend is also reported in our early study of $Sr_2Ir_{1-x}Ru_xO_4$ in which the doping of $Ru^{4+}(4d^4)$ ions offer four $4d$ electrons and a $S = 1$ spin state (see Fig. 5 of Ref. [33]).

Sr_2Ir_{1-x}**Co**$_xO_4$. The Co^{4+} ion carries five $3d$ electrons, thus, assuming the high spin state (one electron per orbital) Hund's rules yield $S = 5/2$ with the orbital angular momentum being completely quenched. It is therefore not surprising that, unlike Fe doping, Co doping readily suppresses the native AFM order, as shown in Figs. 2(d) and 2(e). The Curie-Weiss temperature θ_{CW} decreases drastically from 250 K for

$x = 0$ to 32 K for $x = 0.11$ [see $\Delta\chi^{-1}$ vs T in Fig. 2(d)]. A magnetic peak briefly occurs in a narrow temperature range of 8–10 K for $0.08 \leqslant x < 0.14$, vanishing at $x > 0.14$; it could be either the fading native AFM order or an emergent new magnetic state originating from the interaction between the Co spins. The magnetic state has a vanishing magnetic anisotropy [inset in Fig. 2(e)], implying a weakening SOI effect. Importantly, the effective moment μ_{eff} rises at a fast rate and is accompanied by an equally fast vanishing T_N [Fig. 2(f)]. The closely locked opposite trends of μ_{eff} and T_N as a function of x in Sr_2Ir_{1-x}**Co**$_xO_4$ further strengthens the key notion that it is the value of S of the substituting ion for the Ir ion that predominately determines the magnetic properties in doped Sr_2IrO_4.

C. Electrical resistivity

Despite the vastly different magnetic properties between Sr_2Ir_{1-x}**Fe**$_xO_4$ and Sr_2Ir_{1-x}**Co**$_xO_4$, the transport properties of these compounds exhibit a great deal of similarity,
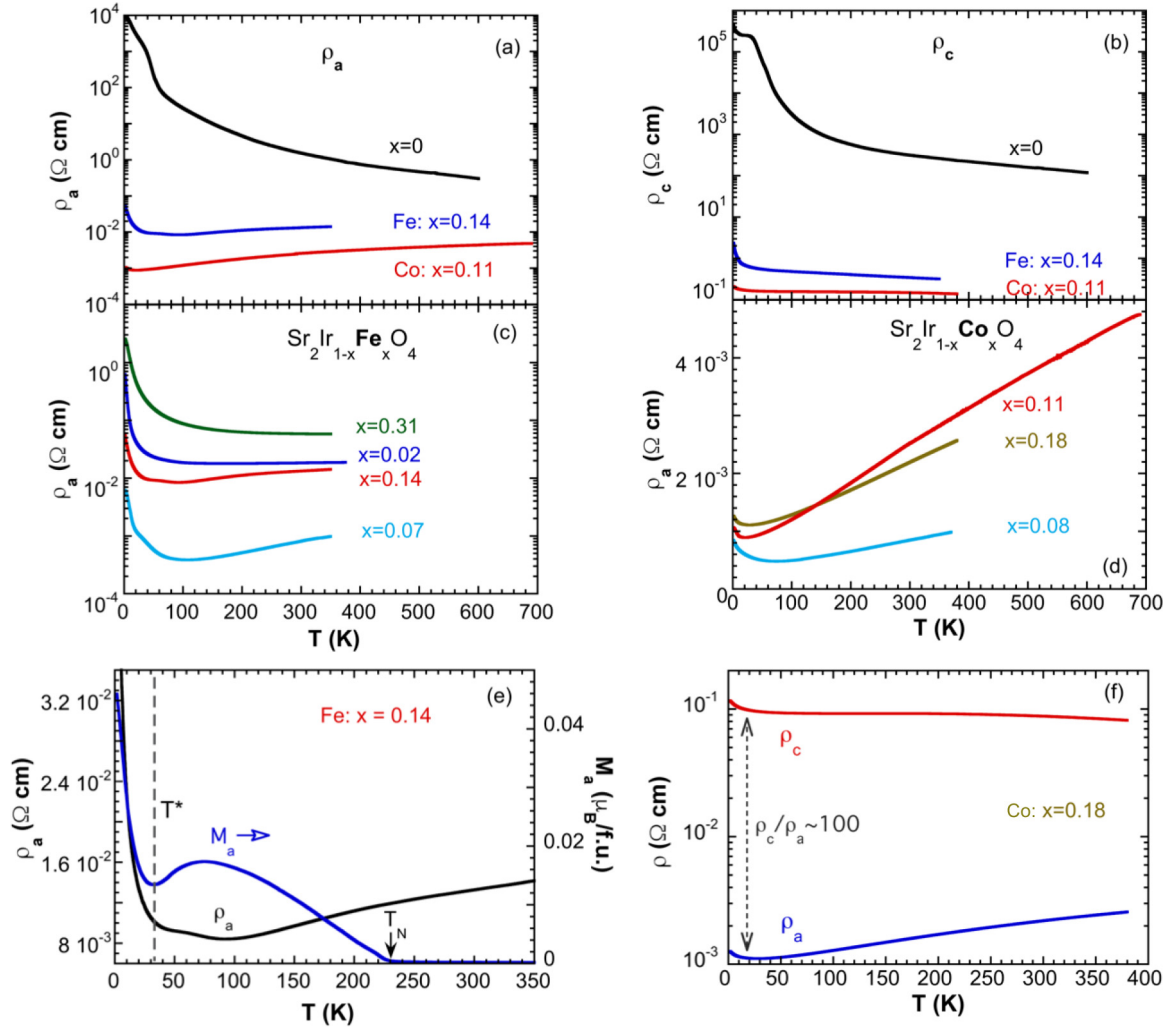
FIG. 3. Transport properties of $Sr_2Ir_{1-x}Fe_xO_4$ and $Sr_2Ir_{1-x}Co_xO_4$: Temperature dependence of the electrical resistivity ρ for $x = 0$ (black), and representative doping $x = 0.11$ of Co (red) and 0.14 of Fe (blue) for (a) the a-axis resistivity ρ_a and (b) the c-axis resistivity ρ_c. Note that the reduction of ρ_a and ρ_c is as much as eight and six orders of magnitude, respectively. Temperature dependence of the a-axis resistivity ρ_a for (c) $Sr_2Ir_{1-x}Fe_xO_4$ and (d) $Sr_2Ir_{1-x}Co_xO_4$. Note ρ_a is as low as 10^{-4} Ω cm for $x = 0.07$ (Fe) and 0.08 (Co). (e) Temperature dependence of the a-axis resistivity ρ_a (left scale) and magnetization M_a (right scale) for $x = 0.14$ of Fe doping and (f) the a-axis resistivity ρ_a and the c-axis resistivity ρ_c for $x = 0.18$ of Co doping.

highlighting a near irrelevance of the magnetic state to the electronic state in Sr_2IrO_4.

As shown in Figs. 3(a) and 3(b), either Fe or Co doping almost instantly delocalizes electrons, drastically reducing the resistivity ρ by up to *eight* orders of magnitude for the a-axis resistivity ρ_a and *six* orders of magnitude for the c-axis resistivity ρ_c. For $Sr_2Ir_{1-x}Fe_xO_4$ the conducting behavior arises from the impurity band generated from the overlap of the extended acceptor bound states, while for $Sr_2Ir_{1-x}Co_xO_4$ the impurity band is due to the percolation of the bound states, a consequence of the scattering off the isoelectronic Co^{4+} impurities. The size of the bound states is of the order of one unit cell, but the percolation limit depends on the neighboring bonds (first, second, third) that have to be considered [40]. It can be calculated straightforwardly for a Bethe lattice of coordination z, $x_{cr} = [z(z-1)]^{-1}$, i.e., for motion in the ab plane $z = 4$ and $x_{cr} \sim 8\%$ and for the three-dimensional

crystal $z = 6$ and $x_{cr} \sim 3\%$. The percolation threshold for Fe is much less than for Co.

It is usual to call "metallic" behavior for positive $d\rho/dT$ and "insulating" behavior for negative slope. In $Sr_2Ir_{1-x}Co_xO_4$, the metallic state exists in a wide temperature range, as shown in Fig. 3(d). The metallic behavior emerges in ρ_a for x as small as 0.08 in both $Sr_2Ir_{1-x}Fe_xO_4$ and $Sr_2Ir_{1-x}Co_xO_4$, where ρ_a drops from 10^4 Ω cm for $x = 0$ to 10^{-4} Ω cm [see Figs. 3(c) and 3(d)]. Note that some resistivity data are collected up to 700 K. In fact, the insulating behavior already vanishes above 100 K at a mere $x = 0.02$ of Fe doping, in which $d\rho_a/dT \sim 0$ [Fig. 3(c)]. However, the c-axis resistivity ρ_c for both Fe and Co doping still exhibits a negative slope of $d\rho_c/dT$ despite the drastically reduced magnitude of ρ_c [Fig. 3(b)]. The contrasting behavior between ρ_a and ρ_c suggests a highly anisotropic metallic state in the materials discussed below.

For $Sr_2Ir_{1-x}Fe_xO_4$, a pronounced upturn in ρ_a and ρ_c below 35 K is closely associated with the magnetic anomaly T^* [Fig. 3(e)] resulting from the spin polarization of the electrons localized in the acceptor band. With increasing Fe doping the interaction between Fe spins becomes larger and so does T^* [Figs. 2(a) and 2(b)]. For N Fe impurities the donor band accommodates up to $2N$ electrons. If the band is spin polarized the up-spin subband is filled and the down-spin subband is empty, i.e., the system is insulating. The recovered insulating behavior for $x = 0.31$ [Fig. 3(b)] is attributed to (weak) localization due to scattering off randomly distributed Fe ions (recall that the isostructural Sr_2FeO_4 is an AFM insulator with a Néel temperature at 60 K [44]). It is interesting to note that the magnetic and transport data of $Sr_2Ir_{1-x}Fe_xO_4$ indicate that the metallic state exists only in a region where the long-range AFM order persists and gives way to a more insulating state when the AFM order vanishes (e.g., $x = 0.31$), hinting unconventional correlation between magnetic and electronic states.

In $Sr_2Ir_{1-x}Co_xO_4$, the metallic state exists in a wide temperature range, as shown in Fig. 3(d). Most remarkably, ρ_a exhibits a pronounced linearity with temperature up to 700 K, with no sign of saturation. Note that for the iridates, the Debye temperature θ_D ranges from 390 to 440 K. The linear-temperature dependence of resistivity at high temperatures is a hallmark of many interesting "bad" metals, such as superconducting cuprates [45] and, more recently, twisted bilayer graphene [46]. High-temperature resistivity of conventional metals, which is driven by strong electron-phonon scattering, saturates at sufficiently high temperatures higher than θ_D when the mean free path of a quasiparticle becomes shorter than the de Broglie wavelength, according to the Boltzmann transport theory. The absence of resistivity saturation suggests a breakdown of conventional theoretical models, and the prevailing view is that this phenomenon is associated with collective fluctuations, possibly spin fluctuations, but the physics of it has remained one of time-honored intellectual challenges [47].

The metallic state is confined to the basal plane. The interplane or c-axis resistivity ρ_c remains having a negative slope of $d\rho_c/dT$ [Fig. 3(b)] for both systems. The anisotropy between ρ_c and ρ_a is large; for example, the ratio $\rho_c/\rho_a \approx 100$ for $x = 0.18$ of Co doping [see Fig. 3(f)]. Similar behavior was observed in the cuprate superconductors, anisotropic organic conductors, and, more recently, in compressed $Sr_3Ir_2O_7$ [48]. In essence, the anisotropic metallic behavior is recognized as a result of confined coherence [49,50]. For the perovskite systems such as the cuprates and the iridates, the single electron coherence is confined to the basal planes so that an interference effect or coherent electron hopping between the basal planes becomes unlikely, thus resulting in *incoherent* nonmetallic transport along the c axis. A confined metallic state can occur only in strongly anisotropic and correlated non-Fermi liquids [50].

D. Specific heat

To evaluate the electronic correlations, we now examine the specific heat $C(T)$, culled in $0.05\,K < T < 50\,K$ for both $Sr_2Ir_{1-x}Fe_xO_4$ and $Sr_2Ir_{1-x}Co_xO_4$. As shown in Fig. 4(a), $C(T)$ for both $x = 0.11$ of Co doping and $x = 0.14$ of Fe

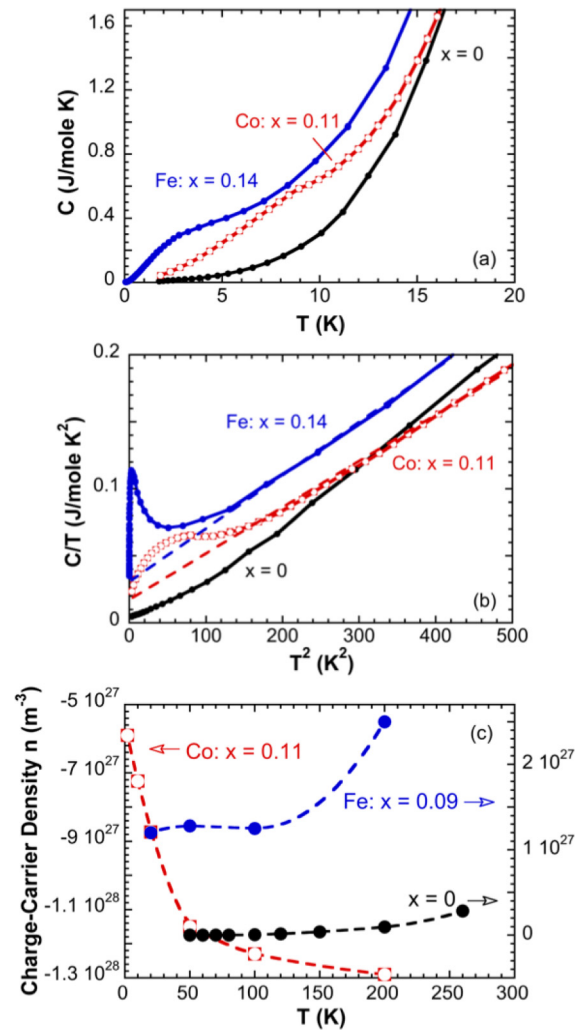FIG. 4. Specific heat and charge-carrier density of $Sr_2Ir_{1-x}Fe_xO_4$ and $Sr_2Ir_{1-x}Co_xO_4$: (a) Temperature dependence of specific heat C and (b) C/T vs T^2 for $x = 0$ (black), 0.11 of Co doping (red), and 0.14 of Fe doping (blue). (c) Temperature dependence of the charge-carrier density n for $x = 0$ (black), 0.09 of Fe doping (blue), and 0.11 of Co doping (red).

doping is not only different but also considerably larger than that for $x = 0$, corroborating the changed ground state. For $x = 0.11$ of Co doping, a weak but visible hump near 10 K in $C(T)$ is attributed to the magnetic order seen in the magnetization [Figs. 2(d) and 2(e)]. On the other hand, $C(T)$ for $x = 0.14$ of Fe doping exhibits no anomaly at T^* near 30 K, but rapidly decreases below 2.5 K, becoming vanishingly small at 0.05 K. The Sommerfeld coefficient, γ, estimated from a plot of $C(T)/T$ vs T^2 is approximately $30\,mJ/mole\,K^2$ for $x = 0.14$ of Fe doping and $19\,mJ/mole\,K^2$ for $x = 0.11$ of Co doping, compared to $4\,mJ/mole\,K^2$ for $x = 0$ [Fig. 4(b); note that γ is extrapolated from the data above the magnetic anomaly marked by the blue and red dashed lines]. The large values of γ for the doped iridates reflect the significant electronic contribution of the emergent metallic state to $C(T)$. Based on the values of γ and the lattice parameters, the effective mass m_{eff} is estimated to be $10.2m_e$ and $5.9m_e$ for the Fe and Co doped samples, respectively (m_e is the electron rest mass).
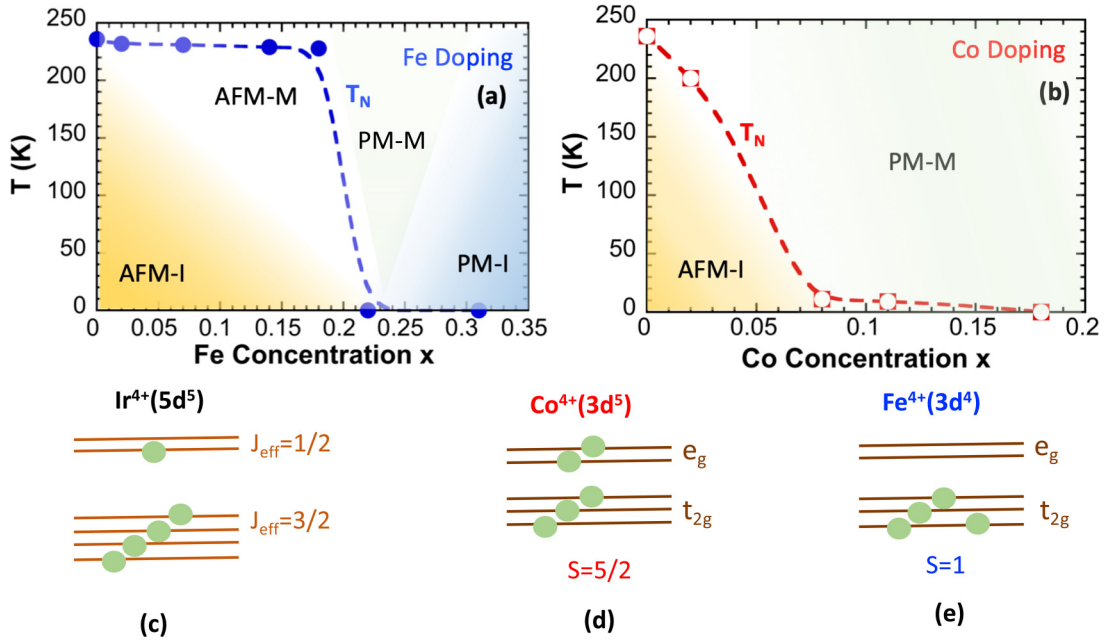
FIG. 5. Phase diagrams for (a) $Sr_2Ir_{1-x}Fe_xO_4$ and (b) $Sr_2Ir_{1-x}Co_xO_4$ generated based on the results, where M = confined metallic state, I = insulating state, and PM = paramagnetism. (c) Schematics of the crystalline field and spin orbit interaction splitting for the $Ir^{4+}(5d^5)$ ions. Schematics of (d) the high spin state (HS) $S = 5/2$ of $Co^{4+}(3d^5)$ impurities and (e) the intermediate spin state (IS) $S = 1$ of $Fe^{4+}(3d^4)$ acceptor impurities.

Furthermore, the Wilson ratio $R_W \sim \chi_o/\gamma$, is 2.7 and 2.6, where $\chi_o = 1.2 \times 10^{-3}$ emu/mole and 7.0×10^{-4} emu/mole for the Fe and Co doped samples, respectively. The significantly enhanced values of both m_{eff} and R_W strongly indicate that electrons are not only highly correlated in $Sr_2Ir_{1-x}Fe_xO_4$ and $Sr_2Ir_{1-x}Co_xO_4$, but also nonlocally correlated, i.e., the impurities interact with each other.

E. Hall effect

The charge-carrier density n, obtained from Hall effect measurements, also indicates a consistent, drastic increase for the Fe and Co doped samples. As shown in Fig. 4(c), the highest absolute values of n at high temperatures increases from $10^{26}/m^3$ for $x = 0$ to $10^{27}/m^3$ and $10^{28}/m^3$ for $x = 0.09$ of Fe doping and $x = 0.11$ of Co doping, respectively, and these values of n are comparable to those of metals, a consequence of the impurity bands. Note that n for Co doped Sr_2IrO_4 is negative, indicating that charge carriers are primarily electrons. Furthermore, the temperature dependence of n for the three compounds is both different and telling. For $x = 0$, n increasing with temperature suggests thermal activation, typical of an insulator or semiconductor. The value of n for $x = 0.09$ of Fe doping is one order of magnitude higher than that for $x = 0$ but its temperature dependence also suggests a significant role of thermal activation; thus, the transport properties are likely governed by both the added holes to the acceptor band and their thermal activation. On the other hand, for $x = 0.11$ of Co doping, the absolute value of n rises initially and then approaches a near saturation above 50 K. This clearly indicates that the transport properties are driven by itinerant electrons in the percolated impurity band, rather than thermally activated.

It is worth mentioning that Sr_2FeO_4 is an antiferromagnetic insulator with $T_N = 60$ K [44] and Sr_2CoO_4 is a ferromagnetic metal with a Curie temperature at 250 K [51]. The physical properties illustrated by $Sr_2Ir_{1-x}Fe_xO_4$ and $Sr_2Ir_{1-x}Co_xO_4$ are fundamentally different from those of Sr_2FeO_4 and Sr_2CoO_4, emphasizing that the phenomena reported here are unique to the title compounds.

IV. CONCLUSIONS

The observations presented in this study provide insight into the iridates. In Fe doped Sr_2IrO_4, a metallic state emerges from the acceptor band as the native AFM order persists—there is no sign of a correlation between the native AFM and insulating states [Fig. 5(a)]. This behavior sharply contrasts that in Co doped Sr_2IrO_4 in which the transport and magnetic properties closely track with each other in a fashion commonly seen in other correlated systems [Fig. 5(b)]. For the Co doped Sr_2IrO_4 the properties arise from the impurity without acceptors or donors. The contrasting behavior suggests that the origin of the AFM-Mott state may have no close association with the electronic conduction state. The absence of a clear correlation between the AFM and Mott in doped Sr_2IrO_4 sharply contrasts that of other correlated materials whose signature is often a strong AFM and Mott correlation.

This study concludes that the distinctly different response of the magnetic state to Fe^{4+} ($3d^4$) and Co^{4+} ($3d^5$) doping is a consequence of the different spin state of the substituting ion for the Ir ion. The impurity bands arising from the percolation of the bound states yield a different metallic behavior in the two systems due to the difference between acceptor states and

charge neutral substitutions. The different electronic configurations of Ir^{4+}, Fe^{4+}, and Co^{4+} are shown in Figs. 5(c)–5(e).

This insight also provides a universal explanation for changes of T_N due to d- or f-electron doping for Ir $5d$ electons in Sr_2IrO_4. The emergent metallic state in Fe or Co doped Sr_2IrO_4 is assisted by the significantly reduced octahedral IrO_6 rotation, which facilitates electron hopping in the basal plane. It is peculiar that the basal plane network of IrO_6, which facilitates coherent electron hopping, is resilient to the high level of doping. These observations may provide a pathway to discoveries of different states in the iridates.

[1] B. J. Kim, H. Jin, S. J. Moon, J. Y. Kim, B. G. Park, C. S. Leem, J. Yu, T. W. Noh, C. Kim, S. J. Oh, J. H. Park, V. Durairaj, G. Cao, and E. Rotenberg, Novel $J_{eff} = 1/2$ Mott State Induced by Relativistic Spin-Orbit Coupling in Sr_2IrO_4, Phys. Rev. Lett. **101**, 076402 (2008).

[2] B. J. Kim, H. Ohsumi, T. Komesu, S. Sakai, T. Morita, H. Takagi, and T. Arima, Phase-sensitive observation of a spin-orbital mott state in Sr_2IrO_4, Science **323**, 1329 (2009).

[3] W. Witczak-Krempa, G. Chen, Y. B. Kim, and L. Balents, Correlated quantum phenomena in the strong spin-orbit regime, Annu. Rev. Condens. Matter Phys. **5**, 57 (2014).

[4] J. G. Rau, E. K. H. Lee, and H. Y. Kee, Spin-orbit physics giving rise to novel phases in correlated systems: iridates and related materials, Annu. Rev. Condens. Matter Phys. **7**, 195 (2016).

[5] G. Cao and P. Schlottmann, The challenge of spin-orbit-tuned ground states in iridates: A Key Issues Review, Rep. Prog. Phys. **81**, 042502 (2018).

[6] G. Jackeli and G. Khaliullin, Mott Insulators in the Strong Spin-Orbit Coupling Limit: From Heisenberg to a Quantum Compass and Kitaev Models, Phys. Rev. Lett. **102**, 017205 (2009).

[7] R. Schaffer, E. K. H. Lee, B. J. Yang, and Y. B. Kim, Recent progress on correlated electron systems with strong spin-orbit coupling, Rep. Prog. Phys. **79**, 094504 (2016).

[8] C. Martins, M. Aichhorn, and S. Biermann, Coulomb correlations in 4d and 5d oxides from first principles-or how spin-orbit materials choose their effective orbital degeneracies, J. Phys.: Condens. Matter **29**, 263001 (2017).

[9] F. Wang and T. Senthil, Twisted Hubbard Model for Sr_2IrO_4: Magnetism and Possible High Temperature Superconductivity, Phys. Rev. Lett. **106**, 136402 (2011).

[10] H. Watanabe, T. Shirakawa, and S. Yunoki, Monte Carlo Study of an Unconventional Superconducting Phase in Iridium Oxide $J_{eff} = 1/2$ Mott Insulators Induced by Carrier Doping, Phys. Rev. Lett. **110**, 027002 (2013).

[11] Z. Y. Meng, Y. B. Kim, and H. Y. Kee, Odd-Parity Triplet Superconducting Phase in Multiorbital Materials with a Strong Spin-Orbit Coupling: Application to Doped Sr_2IrO_4, Phys. Rev. Lett. **113**, 177003 (2014).

[12] Y. Yang, W. S. Wang, J. G. Liu, H. Chen, J. H. Dai, and Q. H. Wang, Superconductivity in doped Sr_2IrO_4: A functional renormalization group study, Phys. Rev. B **89**, 094518 (2014).

[13] Y. K. Kim, N. H. Sung, J. D. Denlinger, and B. J. Kim, Observation of a d-wave gap in electron-doped Sr_2IrO_4, Nat. Phys. **12**, 37 (2016).

[14] A. W. Lindquist and H.-Y. Kee, Odd-parity superconductivity driven by octahedra rotations in iridium oxides, Phys. Rev. B **100**, 054512 (2019).

[15] F. Ye, S. Chi, B. C. Chakoumakos, J. A. Fernandez-Baca, T. Qi, and G. Cao, Magnetic and crystal structures of Sr_2IrO_4:

A neutron diffraction study, Phys. Rev. B **87**, 140406(R) (2013).

[16] G. Cao, J. Bolivar, S. McCall, J. E. Crow, and R. P. Guertin, Weak ferromagnetism, metal-to-nonmetal transition, and negative differential resistivity in single-crystal Sr_2IrO_4, Phys. Rev. B **57**, R11039(R) (1998).

[17] Q. Huang, J. L. Soubeyroux, O. Chmaissem, I. Natali Sora, A. Santoro, R. J. Cava, J. J. Krajewski, and W. F. Peck, Neutron powder diffraction study of the crystal-structures of Sr_2RuO_4 and Sr_2IrO_4 at room-temperature and at 10 K, J. Solid State Chem. **112**, 355 (1994).

[18] R. J. Cava, B. Batlogg, K. Kiyono, H. Takagi, J. J. Krajewski, W. F. Peck, L. W. Rupp, and C. H. Chen, Localized-to-itinerant electron transition in $Sr_2Ir_{1-x}Ru_xO_4$, Phys. Rev. B **49**, 11890 (1994).

[19] M. K. Crawford, M. A. Subramanian, R. L. Harlow, J. A. Fernandez-Baca, Z. R. Wang, and D. C. Johnston, Structural and magnetic studies of Sr_2IrO_4, Phys. Rev. B **49**, 9198 (1994).

[20] Q. Wang, Y. Cao, J. A. Waugh, S. R. Park, T. F. Qi, O. B. Korneta, G. Cao, and D. S. Dessau, Dimensionality-controlled Mott transition and correlation effects in single-layer and bilayer perovskite iridates, Phys. Rev. B **87**, 245109 (2013).

[21] S. Fujiyama, H. Ohsumi, T. Komesu, J. Matsuno, B. J. Kim, M. Takata, T. Arima, and H. Takagi, Two-Dimensional Heisenberg Behavior of $J_{eff} = 1/2$ Isospins in the Paramagnetic State of the Spin-Orbital Mott Insulator Sr_2IrO_4, Phys. Rev. Lett. **108**, 247212 (2012).

[22] J. Dai, E. Calleja, G. Cao, and K. McElroy, Local density of states study of a spin-orbit-coupling induced Mott insulator Sr_2IrO_4, Phys. Rev. B **90**, 041102(R) (2014).

[23] C. Chen, Y. Zhou, X. Chen, T. Han, C. An, Y. Zhou, Y. Yuan, B. Zhang, S. Wang, R. Zhang, L. Zhang, C. Zhang, Z. Yang, L E. DeLong, and G. Cao, Persistent insulating state at megabar pressures in strongly spin-orbit-coupled Sr_2IrO_4, Phys. Rev. B **101**, 144102 (2020).

[24] D. Haskel, G. Fabbris, M. Zhernenkov, P. P. Kong, C. Q. Jin, G. Cao, and M. van Veenendaal, Pressure Tuning of the Spin-Orbit Coupled Ground State in Sr_2IrO_4, Phys. Rev. Lett. **109**, 027204 (2012).

[25] D. Haskel, G. Fabbris, J. H. Kim, L. S. I. Veiga, J. R. L. Mardegan, C. A. Escanhoela, Jr., S. Chikara, V. Struzhkin, T. Senthil, B. J. Kim, G. Cao, and J. W. Kim, Possible Quantum Paramagnetism in Compressed Sr_2IrO_4, Phys. Rev. Lett. **124**, 067201 (2020).

[26] M. Ge, T. F. Qi, O. B. Korneta, D. E. De Long, P. Schlottmann, W. P. Crummett, and G. Cao, Lattice-driven magnetoresistivity and metal-insulator transition in single-layered iridates, Phys. Rev. B **84**, 100402(R) (2011).

[27] H. D. Zhao, J. Terzic, H. Zheng, Y. F. Ni, Y. Zhang, F. Ye and P. Schlottmann, and G. Cao, Decoupling of magnetism and electric transport in single-crystal $(Sr_{1-x}A_x)_2IrO_4$ (A = Ca or Ba), J. Phys.: Condens. Matter **30**, 245801 (2018).

[28] X. Chen, T. Hogan, D. Walkup, W. Zhou, M. Pokharel, M. Yao, W. Tian, T Z. Ward, Y. Zhao, D. Parshall, C. Opeil, J. W. Lynn, V. Madhavan, and S. D. Wilson, Influence of electron doping on the ground state of $(Sr_{1-x}La_x)_2IrO_4$, Phys. Rev. B **92**, 075125 (2015).

[29] T. F. Qi, O. B. Korneta, L. Li, K. Butrouna, V. S. Cao, X. Wan, R. Kaul, and G. Cao, Spin-orbit tuned metal-insulator transitions in single-crystal $Sr_2Ir_{1-x}Rh_xO_4$ $(0 \leqslant x \leqslant 1)$, Phys. Rev. B **86**, 125105 (2012).

[30] S. Calder, G. - X. Cao, M. D. Lumsden, J. W. Kim, Z. Gai, B. C. Sales, D. Mandrus, and A. D. Christianson, Magnetic structural change of Sr_2IrO_4 upon Mn doping, Phys. Rev. B **86**, 220403(R) (2012).

[31] J. C. Wang, S. Aswartham, F. Ye, J. Terzic, H. Zheng, D. Haskel, S. Chikara, Y. Choi, P. Schlottmann, R. Custelcean, S. J. Yuan, and G. Cao, Decoupling of the antiferromagnetic and insulating states in Tb-doped Sr_2IrO_4, Phys. Rev. B **92**, 214411 (2015).

[32] F. Ye, X. Wang, C. Hoffmann, J. C. Wang, S. Chi, M. Matsuda, B. C. Chakoumakos, J. A. Fernandez-Baca, and G. Cao, Structure symmetry determination and magnetic evolution in $Sr_2Ir_{1-x}Rh_xO_4$, Phys. Rev. B **92** 201112(R) (2015).

[33] S. J. Yuan, S. Aswartham, J. Terzic, H. Zheng, H. D. Zhao, P. Schlottmann, and G. Cao, From $J_{eff} = 1/2$ insulator to p-wave superconductor in single-crystal $Sr_2Ir_{1-x}Ru_xO_4$ $(0 \leqslant x \leqslant 1)$, Phys. Rev. B **92**, 245103 (2015).

[34] S. Calder, J. W. Kim, G.-X. Cao, C. Cantoni, A. F. May, H. B. Cao, A. A. Aczel, M. Matsuda, Y. Choi, D. Haskel, B. C. Sales, D. Mandrus, M. D. Lumsden, and A. D. Christianson, Evolution of competing magnetic order in the $J_{eff} = 1/2$ insulating state of $Sr_2Ir_{1-x}Ru_xO_4$, Phys. Rev. B **92**, 165128 (2015).

[35] J. P. Clancy, A. Lupascu, H. Gretarsson, Z. Islam, Y. F. Hu, D. Casa, C. S. Nelson, S. C. LaMarra, G. Cao, and Y.-J. Kim, Dilute magnetism and spin-orbital percolation effects in $Sr_2Ir_{1-x}Rh_xO_4$, Phys. Rev. B **89**, 054409 (2014).

[36] S. Chikara, D. Haske, J.-H. Sim, H.-S. Kim, C.-C. Chen, G. Fabbris, L. S. I. Veiga, N. M. Souza-Neto, J. Terzic, K. Butrouna, G. Cao, M. J. Han, and M. van Veenendal, $Sr_2Ir_{1-x}Rh_xO_4$ $(x < 0.5)$: An inhomogeneous $J_{eff} = 1/2$ hubbard system, Phys. Rev. B **92**, 081114(R) (2015).

[37] L. Zhao, D. H. Torchinsky, H. Chu, V. Ivanov, R. Lifshitz, R. Flint, T. Qi, G. Cao, and D. Hsieh, Evidence of an odd-parity hidden order in a strongly spin-orbit coupled correlated iridates, Nat. Phys. **12**, 32 (2016).

[38] Y. Cao, Q. Wang, J. A. Waugh, T. J. Reber, H. Li, X. Zhou, S. Parham, S.-R. Park, N. C. Plumb, E. Rotenberg, A. Bostwick, J. D. Denlinger, T. Qi, M. A. Hermele, G. Cao, and D. S. Dessau, Hallmarks of the Mott-metal crossover in the hole-doped pseudospin-1/2 Mott insulator Sr_2IrO_4, Nat. Comm. **7**, 11367 (2016).

[39] C. H. Sohn, D.-Y. Cho, C. T. Kuo, L. J. Sandilands, T. F. Qi, G. Cao, and T. W. Noh, X-ray absorption spectroscopy study of the effect of Rh doping in Sr_2IrO_4, Sci. Rep. **6**, 23856 (2016).

[40] P. Schlottmann and C. S. Hellberg, Metal-insulator transition in dirty kondo insulators, J. Appl. Phys. **79**, 6414 (1996).

[41] A. J. Gatimu, R. Berthelot, S. Muir, A. W. Sleight, and M. Subramanian, Synthesis and characterization of $Sr_2Ir_{1-x}M_xO_4$ (M = Ti, Fe, Co) solid solutions, J. Solid State Chem. **190**, 257 (2012).

[42] D. H. Torchinsky, H. Chu, L. Zhao, N. B. Perkins, Y. Sizyuk, T. Qi, G. Cao, and D. Hsieh, Structural Distortion-Induced Magnetoelastic Locking in Sr_2IrO_4 Revealed through Nonlinear Optical Harmonic Generation, Phys. Rev. Lett. **114**, 096404 (2015).

[43] F. Ye, C. Hoffmann, W. Tian, H. Zhao, and G. Cao, Pseudospin-lattice coupling and electric control of the square-lattice iridate Sr_2IrO_4, Phys. Rev. B **102**, 115120 (2020).

[44] S. E. Dann, M. T. Weller, D. B. Currie, M. F. Thomas, and A. D. Al-Rawwas, Structure and magnetic properties of Sr_2FeO_4 and $Sr_3Fe_2O_7$ studied by powder neutron diffraction and Mössbauer spectroscopy, J. Mater. Chem. **3**, 1231 (1993).

[45] V. J. Emery and S. A. Kivelson, Superconductivity in Bad Metals, Phys. Rev. Lett. **74**, 3253 (1995).

[46] H. Polshyn, M. Yankowitz, S. Chen, Y. Zhang, K. Watanabe, T. Taniguchi, C. R. Dean, and A. F. Young, Large linear-in-temperature resistivity in twisted bilayer graphene. Nat. Phys. **15**, 1011 (2019).

[47] J. Zaanen, Why the temperature is high Nature (London) **430**, 512 (2004).

[48] Y. Ding, L. Yang, C.-C. Chen, H.-S. Kim, M. J. Han, W. Luo, Z. Feng, M. Upton, D. Casa, J. Kim, T. Gog, Z. Zeng, G. Cao, H. K. Mao, and M. van Veenendaal, Pressure-Induced Confined Metal from the Mott Insulator $Sr_3Ir_2O_7$, Phys. Rev. Lett. **116**, 216402 (2016).

[49] J. M. Wheatley, T. C. Hsu, and P. W. Anderson, Interlayer pair hopping: Superconductivity from the resonating-valence-bond state, Phys. Rev. B **37**, 5897(R) (1988).

[50] D G. Clarke and S. P. Strong, Confined coherence in strongly correlated anisotropic metals, Adv. Phys. **46**, 545 (1997).

[51] J. Matsuno, Y. Okimoto, Z. Fang, X. Z. Yu, Y. Matsui, N. Nagaosa, H. Kumigashira, M. Oshima, M. Kawasaki, and Y. Tokura, Novel metallic ferromagnet Sr_2CoO_4, Thin Solid Films **486**, 113 (2005).